Preprints of the 21st IFAC World Congress (Virtual)
Berlin, Germany, July 12-17, 2020

Engine-Based Input-Output Linearization for Traction Control Systems ⋆

Elias Reichensdörfer * **Dirk Odenthal** ** **Dirk Wollherr** ***

* *Technical University of Munich, Chair of Automatic Control Engineering, 80333 Munich, Germany and BMW Group, 80788 Munich, Germany (e-mail: elias.reichensdoerfer@bmw.de).*
** *BMW M GmbH, 85748 Garching near Munich, Germany (e-mail: dirk.odenthal@bmw-m.com)*
*** *Technical University of Munich, Chair of Automatic Control Engineering, 80333 Munich, Germany (e-mail: dw@tum.de)*

Abstract: Engine-based traction control marks a paradigm shift for electronic stability systems in the automotive industry. It enables traction control systems with higher bandwidth and performance by an architectural change. As a new approach, only few work exists that considers analytic control design for engine-based traction control. This paper extends our recent work on input-output linearization for engine-based traction control. Global, exponential stability for arbitrary vehicle parameters and time-varying road adhesion coefficients is shown for the first time. Experiments in a test vehicle compare the proposed design with different traction control systems. It is shown that on the considered maneuver, the control design achieves superior tracking performance, disturbance attenuation and damping of drivetrain oscillations.

Keywords: Traction control system, input-output linearization, passivity, zero dynamics.

1. INTRODUCTION

Traction control systems (TCSs) are important for automotive safety as they assist the driver in difficult driving situations, like accelerating on a slippery road or during cornering. This is achieved by adjusting the speed of the accelerated wheels such, that the traction force between road and tire is maximized.

Traditional TCSs partition the control algorithm on the driving dynamics control unit (DCU), which transmits its commands to the engine control unit (ECU). Engine-based traction control is a recent development that partitions the controller directly on the ECU, which reduces communication delay due to synchronization and enables faster computation cycles.

Only few work exists dealing with analytic control design for engine-based TCSs. Jaime et al. (2014) proposed PD control for this purpose, while Zech et al. (2017) used proportional control for active damping. Our recent work, see Reichensdörfer et al. (2018), proposed a complete control design for engine-based TCSs based on input-output linearization, including torsional dynamics of the drivetrain in the design model, cf. also Zech et al. (2018). This ECU-based TCS has been also extended recently to plug-in hybrid electric vehicles (PHEVs) by Zech et al. (2019) and to vehicles with four-wheel drive (4WD) on-demand torque bias systems by Reichensdörfer et al. (2019). While we also presented a detailed stability analysis of the zero dynamics, there still remained some open question, which are addressed within this work.

⋆ This work was supported in part by the BMW Group Driving Dynamics and in part by BMW M.

There already exists different work on input-output linearization for TCSs. Fujii and Fujimoto (2007) use this method based on a 2-state design model and evaluate it in a test vehicle. The same is done by Chapuis et al. (2013), while Nakakuki et al. (2008) put focus on stability analysis of the zero dynamics of the 2-state model. The 2-state model is also used for input-output linearization of anti-lock braking systems (ABSs), for example by Nyandoro et al. (2011) and Mousavi et al. (2018). A detailed analysis of different approaches for both TCSs and ABSs is given in the survey paper by Ivanov et al. (2015).

These approaches however all apply input-output linearization to the widely used 2-state model, which describes the longitudinal speed of the vehicle and the wheel rotational speed only. Also, they do not consider the control architecture explicitly, which however is an important factor in the industry. It is interesting to note that König et al. (2019) proposed a variant of input-output linearization for traction control using the 2-state model in conjunction with a gain scheduling mechanism, stating that performance could be further improved by locating the control algorithm on the ECU.

This paper extends our previous work of applying input-output linearization to a more complex design model with 5 states, including the torsional dynamics of the drivetrain. This leads to an additional damping term in the resulting control law which is shown to be beneficial for traction control. The control algorithm is partitioned on the ECU, evaluated in a test vehicle and compared to both a DCU-based and a benchmark ECU-based TCS. Also, a detailed stability analysis based on parametric Lyapunov functions and passivity is performed, extending our previous results.

2. BACKGROUND

2.1 Modeling of Longitudinal Vehicle Dynamics

The model for the longitudinal vehicle dynamics is taken from our previous published work by Reichensdörfer et al. (2018) and Zech et al. (2018). In state space notation, with state vector $\boldsymbol{x}^T = [x_1\ x_2\ x_3\ x_4\ x_5]$, it is given by

$$\dot{\boldsymbol{x}} = \begin{bmatrix}\dot{x}_1\\ \dot{x}_2\\ \dot{x}_3\\ \dot{x}_4\\ \dot{x}_5\end{bmatrix} = \begin{bmatrix}-x_1/\tau_m\\ x_3/i_G - x_4\\ (x_1 - 2\,T_r/i_G)/J_c\\ (2\,T_r - r_r F_x)/J_r\\ (F_x - F_w)/m\end{bmatrix} + \begin{bmatrix}1/\tau_m\\ 0\\ 0\\ 0\\ 0\end{bmatrix} u\,, \qquad (1)$$

with u the input motor torque in Nm, x_1 the motor torque in Nm, x_2 the twist angle of the crankshaft in rad, x_3 the crankshaft rotational speed in rad/s, x_4 the rotational speed of the rear axle in rad/s and x_5 the longitudinal vehicle speed in m/s. The system output is the crankshaft rotational speed, scaled to wheel level by the total gear ratio i_G as $y = x_3/i_G$. The inertia of the rear axle is J_r, the one of the crankshaft J_c. Further, in (1) we have

$$T_r = k_c x_2 + d_c(x_3/i_G - x_4) \qquad (2a)$$
$$F_x = \mu F_z \sin\big(C_r \arctan(B_r \lambda_x)\big) \qquad (2b)$$
$$F_z = m\, g\, l_f/(l_f + l_r) \qquad (2c)$$
$$\lambda_x = (r_r x_4 - x_5)/v_n \qquad (2d)$$
$$v_n = \max\nolimits_\epsilon(|r_r x_4|_\epsilon, |x_5|_\epsilon) \qquad (2e)$$
$$F_w = (1/2)\rho\, c_w A_{st} x_5 |x_5|\,. \qquad (2f)$$

Here, T_r is the torque on the rear axle, with k_c and d_c stiffness and damping factor of the crankshaft, modeled as torsional spring. Further, F_x is the nonlinear friction force between tire and road, using the tire model by Pacejka (2005), μ the road adhesion coefficient, F_z the normal force on the rear axle, B_r and $C_r \in (1, 2)$ parameters of the Pacejka tire model and τ_m the motor time constant.

The tire force F_x depends further on λ_x, the wheel slip in longitudinal direction, which is the difference of longitudinal speed and rear axle rotational speed, scaled by the tire radius r_r, divided by the normalization velocity. This velocity, here denoted with v_n, is the absolute maximum of $r_r x_4$ and x_5 and is typically modified in literature, cf. Rill (2007), in order to avoid zero denominator in (2d). We use our previously proposed modification, given by $\max(a, b) \approx \max_\epsilon(a, b) = (1/2)(a + b + |a - b|_\epsilon)$ and $|a| \approx |a|_\epsilon = \sqrt{a^2 + \epsilon}$ with $\epsilon > 0$, so $v_n > 0$. This method avoids division by zero for $x_4 = x_5 = 0$ and instead produces $\lambda_x = F_x = 0$ in this case, which makes sense physically, as in standstill no longitudinal force is generated. Also, it keeps F_x continuously differentiable and produces accurate results in simulation of standard maneuvers for TCSs, see Reichensdörfer et al. (2018) and Zech et al. (2018) for a model validation and numerical parameters.

Finally, the normal force F_z depends on the vehicle mass m, gravitational constant g and the lever arm as a function of the distance between the vehicle center of gravity and its rear axle l_r, respectively front axle l_f. The aerodynamic drag force F_w depends on air density ρ, vehicle front surface area A_{st} and aerodynamic drag coefficient c_w. All vehicle parameters are assumed to be strictly positive.

In the following, the control design for TCSs using engine-based input-output linearization is restated.

2.2 Engine-Based Input-Output Linearization for TCSs

Using the method of input-output linearization by Isidori (1989), cf. also Byrnes and Isidori (1989), differentiating the system output y twice results in

$$\ddot{y} = \frac{1}{i_G J_c}\Big[\frac{1}{\tau_m}\Big(u - x_1\Big) - \frac{2}{i_G}\Big(k_c\dot{x}_2 + d_c\Big(\frac{\dot{x}_3}{i_G} - \dot{x}_4\Big)\Big)\Big]\,. \qquad (3)$$

Since the system input u appears in (3), it can be solved for the linearizing input by defining $\ddot{y} = v$ as input to the linearized substitute system. This control input is

$$u = x_1 + \tau_m\Big[v J_c i_G + \frac{2}{i_G}\Big(k_c\dot{x}_2 + d_c\Big(\frac{\dot{x}_3}{i_G} - \dot{x}_4\Big)\Big)\Big]\,. \qquad (4)$$

The state transformation $\boldsymbol{\phi} : \mathbb{R}^5 \mapsto \mathbb{R}^5$, mapping from $\boldsymbol{x}$ to $\boldsymbol{\xi}$-coordinates, with $\boldsymbol{\xi}^T = [\xi_1\ \xi_2\ \xi_3\ \xi_4\ \xi_5]$ and

$$\boldsymbol{\xi} = \boldsymbol{\phi}(\boldsymbol{x}) = \begin{bmatrix}\phi_1(\boldsymbol{x})\\ \phi_2(\boldsymbol{x})\\ \phi_3(\boldsymbol{x})\\ \phi_4(\boldsymbol{x})\\ \phi_5(\boldsymbol{x})\end{bmatrix} = \begin{bmatrix}x_3/i_G\\ (i_G x_1 - 2\,T_r)/(J_c i_G^2)\\ x_2\\ x_4\\ x_5\end{bmatrix} \qquad (5)$$

can be used, together with the inverse transformation,

$$\boldsymbol{x} = \boldsymbol{\phi}^{-1}(\boldsymbol{\xi}) = \begin{bmatrix}\phi_1^{-1}(\boldsymbol{\xi})\\ \phi_2^{-1}(\boldsymbol{\xi})\\ \phi_3^{-1}(\boldsymbol{\xi})\\ \phi_4^{-1}(\boldsymbol{\xi})\\ \phi_5^{-1}(\boldsymbol{\xi})\end{bmatrix} = \begin{bmatrix}i_G J_c \xi_2 + 2\,T_r/i_G\\ \xi_3\\ i_G\xi_1\\ \xi_4\\ \xi_5\end{bmatrix}, \qquad (6)$$

to obtain the system in Byrnes-Isidori normal form. To derive the resulting zero dynamics, set $\xi_1 = \xi_2 = v = 0$ and insert the expression for u from (4). Note that T_r in (6) is expressed as $T_r = k_c\xi_3 + d_c(\xi_1 - \xi_4)$ in $\boldsymbol{\xi}$-coordinates. Define $\boldsymbol{z}^T = [z_1\ z_2\ z_3] = [\xi_3\ \xi_4\ \xi_5]$ to get

$$\dot{\boldsymbol{z}} = \begin{bmatrix}\dot{z}_1\\ \dot{z}_2\\ \dot{z}_3\end{bmatrix} = \begin{bmatrix}-z_2\\ \big(2(k_c z_1 - d_c z_2) - r_r F_x\big)/J_r\\ (F_x - F_w)/m\end{bmatrix}, \qquad (7)$$

which are the zero dynamics of the system (1). This procedure has been applied to derive an engine-based TCS by Reichensdörfer et al. (2018), where it was shown that (7) is globally asymptotically stable for all vehicle parameters and constant road adhesion coefficients, while the performance of the TCS was verified in experiments. However, some open questions remained, which can be stated as follows.

2.3 Problem Statement

Overall, there are three open research questions that this paper aims to address:

(1) Are the zero dynamics (7) exponentially stable?
(2) How compares (4) to traditional DCU-based TCSs?
(3) How compares (4) to other ECU-based TCSs?

Item 1 is of interest for safety critical systems like TCSs, as exponential stability not only guarantees that the system trajectories are stable and decay to zero eventually, but also decay to zero "fast". Also, stability for time-varying road adhesion coefficients has not been proved formally yet, which is of interest for realistic road conditions.

Items 2 and 3 are of practical interest. While item 3 was evaluated in our previous work using sensitivity functions and simulation, experimental validation is still missing. Hence, this work closes these gaps.

3. METHODS

3.1 Passivity and Absolute Stability Considerations

One interesting fact about the zero dynamics (7) is, that they can be expressed as a Lur'e system, as introduced by Lur'e and Postnikov (1944), by $\dot{\boldsymbol{z}} = \boldsymbol{A}\boldsymbol{z} + \boldsymbol{B}\boldsymbol{u}$, $\boldsymbol{y} = \boldsymbol{C}\boldsymbol{z}$, $\boldsymbol{y}^T = [y_1\ y_2]$, $\boldsymbol{u}^T = [u_1\ u_2]$, with $\boldsymbol{u} = -\boldsymbol{\psi}(\boldsymbol{y})$ and

$$\dot{\boldsymbol{z}} = \begin{bmatrix} 0 & -1 & 0 \\ 2k_c/J_r & -2d_c/J_r & 0 \\ 0 & 0 & 0 \end{bmatrix} \boldsymbol{z} + \begin{bmatrix} 0 & 0 \\ r_r/J_r & 0 \\ -1/m & 1/m \end{bmatrix} \boldsymbol{u} \tag{8a}$$

$$\boldsymbol{y} = \begin{bmatrix} 0 & r_r & 0 \\ 0 & 0 & 1 \end{bmatrix} \boldsymbol{z}\,,\ \boldsymbol{\psi}(\boldsymbol{y}) = \begin{bmatrix} \psi_1(y_1, y_2, t) \\ \psi_2(y_2) \end{bmatrix} = \begin{bmatrix} F_x \\ F_w \end{bmatrix}. \tag{8b}$$

Assuming $0 < \mu_{\min} \leq \mu(t) \leq \mu_{\max} < \infty\, \forall t \in \mathbb{R}_0^+$, (8a) and (8b) describe a linear time-invariant (LTI) system in negative feedback with a sector-bounded, time-varying, 2-dimensional nonlinearity. The longitudinal slip stiffness of the tire is $c_x = \mu F_z B_r C_r$ and $\lambda_x \in (-2, 2)$ by (2d), so the bounds for F_x are $\underline{c}_x = (1/2)\mu_{\min} F_z \sin\big(C_r \arctan(2\, B_r)\big)$, $\bar{c}_x = \mu_{\max} F_z B_r C_r$, with $(F_x - \underline{c}_x\lambda_x)(F_x - \bar{c}_x\lambda_x) \leq 0$.

It can be noted that the Kalman conjecture does not apply here. While it is known due to Barabanov (1988) that the conjecture is true for systems of order $n = 3$ (and false due to Fitts (1966) for $n \geq 4$), it requires a single-input, single-output LTI system in feedback with a monotone, scalar nonlinearity, which is not the case for (8a)-(8b).

A common way to analyze systems like (8a)-(8b) is the Kalman-Yakubovich-Popov Lemma, cf. Khalil (1996), which states that if $\exists \boldsymbol{P} = \boldsymbol{P}^T \succ 0$ such that

$$\boldsymbol{A}^T\boldsymbol{P} + \boldsymbol{P}\boldsymbol{A} \preceq 0 \text{ and } \boldsymbol{P}\boldsymbol{B} = \boldsymbol{C}^T\,, \tag{9}$$

then the corresponding linear system is positive real (passive), denoting with $\succ, \prec, \succeq, \preceq$ positive/negative (semi) definiteness. Here, the linear part is not passive, because $\boldsymbol{P}\boldsymbol{B} = \boldsymbol{C}^T$ results in contradicting conditions.

Choosing a slightly different, less obvious formulation with

$$\hat{\boldsymbol{y}} = \begin{bmatrix} \hat{y}_1 \\ \hat{y}_2 \end{bmatrix} = \begin{bmatrix} 0 & r_r & -1 \\ 0 & 0 & 1 \end{bmatrix} \boldsymbol{z} \tag{10}$$

and v_n a function of $(\hat{y}_1 + \hat{y}_2, \hat{y}_2)$ instead of (y_1, y_2), so that $\lambda_x = \hat{y}_1/v_n$ instead of $\lambda_x = (y_1 - y_2)/v_n$, gives an LTI system for which (9) admits the unique solution

$$\boldsymbol{P} = \operatorname{diag}(2k_c, J_r, m)\,. \tag{11}$$

This is not sufficient to show exponential stability of (7), as will be shown in the following. The next step is usually to apply loop transformations to the Lur'e system in order to compensate shortage of passivity in one channel with excess of passivity in another channel, cf. Khalil (1996).

Here, only $\hat{y}_1$ can be used for output feedback of the LTI part, since $\lim_{z_3 \to 0} \partial F_w/(\partial z_3) = 0$. This results, with $k_1 > 0$, in the following passivity condition

$$(r_r z_2 - z_3)F_x - k_1(r_r z_2 - z_3)^2 + z_3 F_w \geq 0\,. \tag{12}$$

However, no such k_1 can exist if global stability is of interest and (z_2, z_3) can get arbitrarily large. Limiting (z_2, z_3) to practical ranges, cf. Adamy (2014), makes decay rates depend on these ranges, which is undesirable. Input-feedforward on the other hand introduces a feed-through term in (10), which complicates symbolic analyses.

Therefore, we propose a different approach that combines these new passivity-based findings with our previous work.

3.2 Stability Analysis of Wheel-Slip Zero Dynamics

Considering the parametric Lyapunov function candidate

$$V_s(\boldsymbol{z}) = \frac{1}{2}\boldsymbol{z}^T\boldsymbol{P}\boldsymbol{z} = \frac{1}{2}(2k_c z_1^2 + J_r z_2^2 + m z_3^2) \tag{13}$$

obtained from (11). Calculation of its time derivative gives

$$\dot{V}_s(\boldsymbol{z}, t) = -2d_c z_2^2 - z_3 F_w - (r_r z_2 - z_3)F_x \tag{14a}$$

$$= -2d_c z_2^2 - z_3 F_w - v_n \lambda_x F_x\,, \tag{14b}$$

and since $\lambda_x F_x \geq 0 \Rightarrow \dot{V}_s(\boldsymbol{z}, t) \preceq 0$, so the zero dynamics are Lyapunov stable. Asymptotic stability was shown by Reichensdörfer et al. (2018) using a more complicated, parametric Lyapunov function which included a mixed term for z_1 and z_2. Asymptotic stability can also be shown by LaSalle's invariance principle, when assuming that μ is constant, as then $\dot{V}_s(\boldsymbol{z}, t) = \dot{V}_s(\boldsymbol{z}) = 0 \iff z_2 = z_3 = 0$, but then also $\dot{z}_2 = (2k_c/J_r)z_1 \neq 0$ for $z_1 \neq 0$, so $\dot{V}_s(\boldsymbol{z}) = 0$ can only be maintained by the zero solution.

However, the question if the zero dynamics are also exponentially stable has not been considered yet. We show in the following that the zero dynamics are globally exponentially stable for bounded, time-varying $\mu(t)$, arbitrary vehicle parameters and arbitrary sector bounded tire force nonlinearities. This provides stronger stability and robustness guarantees than previous work.

In order to show exponential stability, we combine the herein proposed Lyapunov function (13) with the Lyapunov function we previously proposed, given by

$$V_c(\boldsymbol{z}) = p_{11}z_1^2 + p_{22}z_2^2 + p_{33}z_3^2 - z_1 z_2 \tag{15}$$

with parameter dependent coefficients defined as

$$p_{11} = \frac{\bar{c}_x d_c r_r^2 + 48 J_r k_c \sqrt{\epsilon} + 12 d_c^2 \sqrt{\epsilon}}{12 J_r d_c \sqrt{\epsilon}} \tag{16a}$$

$$p_{22} = \frac{\bar{c}_x d_c r_r^2 + 48 J_r k_c \sqrt{\epsilon}}{24 d_c k_c \sqrt{\epsilon}} \tag{16b}$$

$$p_{33} = (m/J_r)p_{22}\,. \tag{16c}$$

It was shown by Reichensdörfer et al. (2018) that (15) is positive definite for all vehicle parameters and that its time derivative, given by

$$\dot{V}_c(\boldsymbol{z}, t) = \dot{V}_{c1}(\boldsymbol{z}) + \dot{V}_{c2}(\boldsymbol{z}, t) \tag{17a}$$

$$\dot{V}_{c1}(\boldsymbol{z}) = -q_1 z_1^2 - q_2 z_2^2 - q_3 z_3^2 |z_3| \tag{17b}$$

$$\dot{V}_{c2}(\boldsymbol{z}, t) = -q_4 v_n \lambda_x F_x + q_5 z_1 F_x \tag{17c}$$

with the coefficients of $\dot{V}_{c1}$ and $\dot{V}_{c2}$ defined as

$$q_1 = 2k_c/J_r\,,\quad q_2 = 7 + (d_c \bar{c}_x r_r^2)/(6k_c J_r \sqrt{\epsilon})\,,$$
$$q_3 = \rho c_w A_{st}(\bar{c}_x d_c r_r^2 + 48 J_r k_c \sqrt{\epsilon})/(24 k_c d_c J_r \sqrt{\epsilon})\,,$$
$$q_4 = 4/d_c + \bar{c}_x r_r^2/(12 J_r k_c \sqrt{\epsilon})\,,\quad q_5 = r_r/J_r\,,$$

is negative definite. Two difficulties arise when trying to strengthen the results from asymptotic stability and constant μ to exponential stability with time-varying μ. First, as (14b) does not contain a z_1 term, neither exponential, nor asymptotic stability can be concluded using V_s. Also, both LaSalle's invariance principle and Barbalat's Lemma cannot be applied, since μ is time-varying and might not be uniformly continuous. Second, as the $z_3^2|z_3|$ term is effectively cubic in z_3, its exponent does not match the exponents of V_s, V_c, which are both quadratic. Therefore, exponential stability cannot be concluded directly.

While $\dot{V}_c$ does contain the quadratic term $-q_1 z_1^2$, it cannot be used directly for constructing an upper bound, as the original proof uses this term to partially compensate the indefinite $q_5 z_1 F_x$ term in (17c). Hence, we first resolve this by a slight modification of the original proof.

Theorem 1. *The zero dynamics are globally asymptotically stable for all vehicle parameters and bounded positive time-varying road adhesion coefficients $\mu(t)$.*

Proof. Define the parametric scaling factor η by

$$\eta = \frac{\bar{c}_x d_c r_r^2}{\bar{c}_x d_c r_r^2 + 6 J_r k_c \sqrt{\epsilon}} \in (0,1) \tag{18}$$

and redefine (17a) to $\dot{V}_c(\boldsymbol{z},t) = \dot{V}_{c3}(\boldsymbol{z}) + \dot{V}_{c4}(\boldsymbol{z},t)$ with

$$\dot{V}_{c3}(\boldsymbol{z}) = -q_1(1-\eta)z_1^2 - q_2 z_2^2 - q_3 z_3^2|z_3| \tag{19a}$$

$$\dot{V}_{c4}(\boldsymbol{z},t) = -q_4 v_n \lambda_x F_x + q_5 z_1 F_x - q_1 \eta z_1^2 \,. \tag{19b}$$

The rest follows analogously to the original proof: $\dot{V}_{c4}(\boldsymbol{z},t) = 0$ is a quadratic equation in z_1 with discriminant d_{z_1}

$$d_{z_1} = -\eta\Big(\frac{32k_c}{d_c J_r} + \frac{2\bar{c}_x r_r^2}{3J_r^2\sqrt{\epsilon}}\Big) v_n \lambda_x F_x + \frac{r_r^2}{J_r^2} F_x^2 \tag{20a}$$

$$\leq -\eta\Big(\frac{32k_c}{d_c J_r} + \frac{2\bar{c}_x r_r^2}{3J_r^2\sqrt{\epsilon}}\Big) v_n \lambda_x F_x + \frac{r_r^2}{J_r^2} \bar{c}_x \lambda_x F_x \,, \tag{20b}$$

and w.l.o.g. assume $\lambda_x \neq 0 \Rightarrow F_x \neq 0$, so if (20b) < 0 then $\lambda_x F_x$ can be canceled out from (20b). Finally, using $v_n \geq 3\sqrt{\epsilon}/2$, we get $d_{z_1} \leq -42\eta k_c\sqrt{\epsilon}/(d_c J_r) < 0$, so $\dot{V}_{c4}(\boldsymbol{z},t) = 0$ has no real solutions and $\dot{V}_{c4}(\boldsymbol{z},t) \leq 0$. Furthermore, $\dot{V}_c(\boldsymbol{z},t) \leq \dot{V}_{c3}(\boldsymbol{z}) \prec 0$ and since $V_c(\boldsymbol{z}) \succ 0$ does not depend on time explicitly, global asymptotic stability for all parameters and time-varying μ follows. □

Remark 1. *The original proof used $\eta = 1$, which gives also a time invariant $\dot{V}_{c3}$ as in (19a), however without the z_1^2 term, which is required for exponential stability and for time-varying adhesion coefficients. Theorem 1 solves this by shifting only a large enough portion of the $-q_1 z_1^2$ term from $\dot{V}_{c1}$ to $\dot{V}_{c2}$ in order to construct $\dot{V}_{c3}$ and $\dot{V}_{c4}$.*

However, this still does not resolve the problem that the $-q_3 z_3^2|z_3|$ term in $\dot{V}_{c3}$ is not quadratic. In order to address this, we define the new Lyapunov function

$$V(\boldsymbol{z}) = V_s(\boldsymbol{z}) + V_c(\boldsymbol{z}) \,, \tag{21}$$

which is positive definite since V_s and V_c are positive definite. After some rearrangements, its time-derivative is derived as

$$\dot{V}(\boldsymbol{z},t) = \dot{V}_1(\boldsymbol{z},t) + \dot{V}_2(\boldsymbol{z},t) \tag{22a}$$

$$\dot{V}_1(\boldsymbol{z},t) = -\tilde{q}_1 z_1^2 - \tilde{q}_2 z_2^2 - \tilde{q}_3 z_3^2|z_3| - v_n\lambda_x F_x \tag{22b}$$

$$\dot{V}_2(\boldsymbol{z},t) = -q_2 z_2^2 - q_3 z_3^2|z_3| + \dot{V}_{c4}(\boldsymbol{z},t) \tag{22c}$$

with $\tilde{q}_1 = q_1(1-\eta)$, $\tilde{q}_2 = 2d_c$ and $\tilde{q}_3 = (1/2)\rho c_w A_{st}$. Since $\dot{V}_2(\boldsymbol{z},t) \leq 0$, it would suffice for exponential stability to show that $\dot{V}_1(\boldsymbol{z},t) \leq -W(\boldsymbol{z}) \prec 0$ for some positive definite quadratic form $W(\boldsymbol{z})$.

Remark 2. *Since for $z_3 \to 0$, the $-\tilde{q}_3 z_3^2|z_3|$ term vanishes faster than any quadratic, no such W can exist if only the first three terms in (22b) would be considered. In the following, it is shown how the $-v_n\lambda_x F_x$ term can be used to guarantee exponential stability nevertheless.*

We can now state the main stability result of this work.

Theorem 2. *The zero dynamics are globally exponentially stable for all vehicle parameters and bounded positive time-varying road adhesion coefficients $\mu(t)$.*

Proof. Since $\underline{c}_x|\lambda_x| \leq |F_x|$, so $\dot{V}_1(\boldsymbol{z},t) \leq -\dot{U}_1(\boldsymbol{z})$ with

$$\dot{U}_1(\boldsymbol{z}) = \tilde{q}_1 z_1^2 + \tilde{q}_2 z_2^2 + \tilde{q}_3 z_3^2|z_3| + \underline{c}_x(r_r z_2 - z_3)^2/v_n \,. \tag{23}$$

Because $\underline{c}_x$ is constant, compare section 3.1, the function $\dot{U}_1(\boldsymbol{z})$ does not depend on time explicitly and it remains to show that

$$\dot{U}_1(\boldsymbol{z}) \geq W(\boldsymbol{z}) \tag{24}$$

with $W(\boldsymbol{z}) = \alpha_1 z_1^2 + \alpha_2 z_2^2 + \alpha_3 z_3^2$, so a necessary condition is $\alpha_1 \leq \tilde{q}_1$ and $\alpha_2 \leq \tilde{q}_2$. First, assume that $(z_2,z_3) \in \mathbb{R}^2 \setminus (-1,1)^2$. If $|z_3| \geq 1 \Rightarrow \tilde{q}_3 z_3^2|z_3| \geq \alpha_3 z_3^2$ with $\alpha_3 \leq \tilde{q}_3$. If $|z_3| < 1$ and $|z_2| \geq 1$ then it is required that

$$\tilde{q}_2 z_2^2 + \tilde{q}_3 z_3^2|z_3| \geq \alpha_2 z_2^2 + \alpha_3 z_3^2 \tag{25a}$$

$$\Rightarrow \tilde{q}_2 z_2^2 \geq \alpha_2 z_2^2 + \alpha_3 z_3^2 \text{ as } |z_3| < 1, |z_2| \geq 1 \tag{25b}$$

$$\Rightarrow (\tilde{q}_2 - \alpha_2) z_2^2 \geq \alpha_3 z_3^2 \tag{25c}$$

$$\Rightarrow (\tilde{q}_2 - \alpha_2) \geq \alpha_3 \,. \tag{25d}$$

Inequality (25b) must hold since the $\tilde{q}_3 z_3^2|z_3|$ term vanishes faster than the quadratic terms. Inequality (25d) follows by minimizing over $|z_2| \geq 1$ and maximizing over $|z_3| \leq 1$ to ensure the inequality holds in the "worst case" when $|z_2| = |z_3| = 1$. Thus, (24) holds for $z_1 \in \mathbb{R}$ and $(z_2,z_3) \in \mathbb{R}^2 \setminus (-1,1)^2$ if $\alpha_1 \leq \tilde{q}_1$, $\alpha_2 + \alpha_3 \leq \tilde{q}_2$ and $\alpha_3 \leq \tilde{q}_3$.

Next, consider the more interesting case when $z_1 \in \mathbb{R}$ and $(z_2,z_3) \in [-1,1]^2$. Within this domain, v_n can be bounded by a constant like $v_n \leq \tilde{v}_n$ with

$$\tilde{v}_n = \max\nolimits_\epsilon(|r_r|_\epsilon, |1|_\epsilon) \,. \tag{26}$$

Now, with $\tilde{q}_4 = \underline{c}_x/\tilde{v}_n > 0$ and $(z_2,z_3) \in [-1,1]^2$, (24) can be bounded by $\dot{U}_1(\boldsymbol{z}) \geq \dot{U}_2(\boldsymbol{z})$ with

$$\dot{U}_2(\boldsymbol{z}) = \tilde{q}_1 z_1^2 + \tilde{q}_2 z_2^2 + \tilde{q}_3 z_3^2|z_3| + \tilde{q}_4(r_r z_2 - z_3)^2 \,, \tag{27}$$

so if $\dot{U}_2(\boldsymbol{z}) \geq W(\boldsymbol{z})$ then also (24) holds. Expand the last term in (27) and rewrite $\delta\dot{U}_2(\boldsymbol{z}) = \dot{U}_2(\boldsymbol{z}) - W(\boldsymbol{z})$ as

$$\delta\dot{U}_2(\boldsymbol{z}) = (\tilde{q}_1 - \alpha_1) z_1^2 + [z_2 \;\; z_3]\, \boldsymbol{Q} \begin{bmatrix} z_2 \\ z_3 \end{bmatrix} + \tilde{q}_3 z_3^2|z_3| \,, \tag{28a}$$

$$\boldsymbol{Q} = \begin{bmatrix} \tilde{q}_4 r_r^2 + (\tilde{q}_2 - \alpha_2) & -\tilde{q}_4 r_r \\ -\tilde{q}_4 r_r & (\tilde{q}_4 - \alpha_3) \end{bmatrix} . \tag{28b}$$

Now the problem reduces to finding conditions on α_2, α_3 such that $\boldsymbol{Q} \succ 0$ and for which also the previous derived necessary inequalities still hold. These conditions can be obtained by the two principal minors of $\boldsymbol{Q}$, given by

$$\Delta_1 = \tilde{q}_4 r_r^2 + \tilde{q}_2 - \alpha_2 > 0 \tag{29a}$$

$$\Delta_2 = \tilde{q}_2\tilde{q}_4 + \alpha_2\alpha_3 - \tilde{q}_4\alpha_2 - \tilde{q}_2\alpha_3 - \tilde{q}_4 r_r^2 \alpha_3 > 0 \,. \tag{29b}$$

Condition (29a) can be ensured by taking $\alpha_2 \leq \tilde{q}_2$, which is already implicitly required by (25d). For condition (29b), it is clear that by making α_2 and α_3 small enough that $\Delta_2 \approx \tilde{q}_2\tilde{q}_4 > 0$ can be enforced with arbitrary accuracy. Therefore, there always exist α_1, α_2, $\alpha_3 > 0$ such that $\boldsymbol{Q} \succ 0$ and additionally $\alpha_1 \leq \tilde{q}_1$, $\alpha_2 + \alpha_3 \leq \tilde{q}_2$ and $\alpha_3 \leq \tilde{q}_3$. Hence, the origin is globally exponentially stable for all vehicle parameters and for bounded positive time-varying road adhesion coefficients. □

Combining the passivity based V_s with V_c in (21) enabled us to proof Theorem 2, while keeping coefficients simple, thus solving item 1 from section 2.3. We proceed with an additional experimental evaluation of the proposed TCS.

4. EXPERIMENTS

Experimental validation is done in a test vehicle, where the ECU-based controllers are implemented prototypical on an embedded real-time system, bypassing the commands of the standard, DCU-based TCS with a sample time of 10 ms. The proposed controller (4) is implemented as by Reichensdörfer et al. (2018), where the $x_3/i_G - x_4$ term can be interpreted as differential speed, damped by a PD controller with proportional gain $2\tau_m k_c/i_G$ and derivative gain $2\tau_m d_c/i_G$ and filter time constant of 20 ms. The target speed generation is out of the scope of this work and assumed to be provided by a higher level controller. By default, the controller is turned off (the driver is the controller then) and only if the actual engine speed exceeds the target speed, the TCS is activated. The input v in (4) is generated by the reference model

$$v = -(1/\tau_m)\dot{y} + i_G w/(\tau_m J_r) \tag{30}$$

where $\dot{y}$ is also estimated using a derivative filter of the measured y signal and w is the reference model input generated by a PID controller, taking the deviation between target and actual engine speed as input. The PID controller was tuned in experiments using the Ziegler-Nichols tuning rules and included an anti-windup mechanism to account for actuator saturation.

This control design is compared to a standard DCU-based TCS and also to a benchmark implementation of an ECU-based TCS. The benchmark is an ECU-based PI controller, combined with a fine-tuned disturbance observer that is used for feedforward control. The considered maneuver is a longitudinal acceleration from almost standstill, with an abrupt change in the road adhesion coefficient changing from dry asphalt ($\mu \approx 1$) to a watered metal plate ($\mu \approx 0.1$), which at the end changes back again to dry asphalt.

The results of the three considered TCSs on this maneuver are depicted in figure 1, where the approximate start and end points of the watered metal plate are indicated with vertical, black, dashed lines. Figure 1a shows the results of the DCU-based TCS, where around $t \approx 2$ s the road adhesion coefficient drops to $\mu \approx 0.1$ and at around $t \approx 12$ s raises back to $\mu \approx 1$ again. The DCU-based TCS is able to stabilize the longitudinal dynamics but shows a large overshoot after the initial change in μ and oscillates during driving on the low friction underground.

Figure 1b shows the results of the ECU-based benchmark controller. Due to higher bandwidth of this architecture, the over shot at $t \approx 2$ s is significantly lower than for the DCU-based TCS. However, this design requires approximately one additional second to track the target speed with a small error only after $t \approx 4$ s. Also, at $t \approx 10$ s, the engine speed starts to oscillate such that the maneuver is interrupted at $t \approx 12$ s, indicating a lack of robustness to varying μ. Finally, figure 1c shows the results of the ECU-based TCS using input-output linearization. The overshoot at $t \approx 3$ s is 21% smaller than for the benchmark and the controller almost immediately tracks the target speed without visible oscillations. Also, the acceleration at $t \approx 11$ s on $\mu \approx 1$ shows no oscillations, despite the highly nonlinear disturbance.

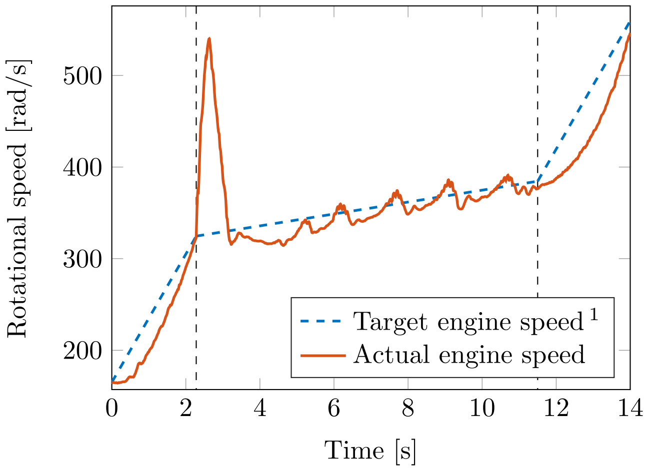

(a) Traditional DCU-based traction control.

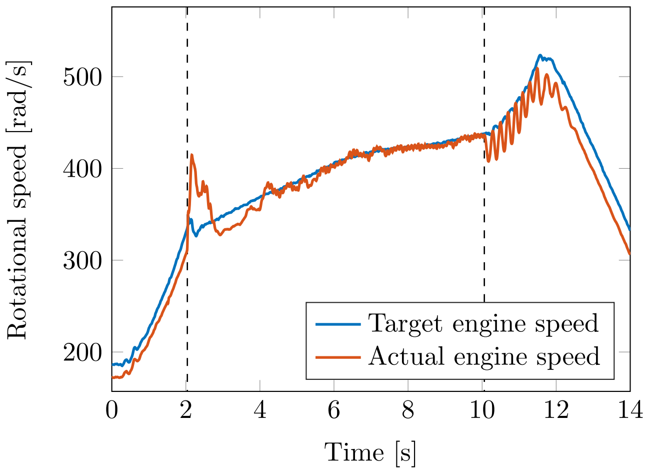

(b) Benchmark for ECU-based traction control.

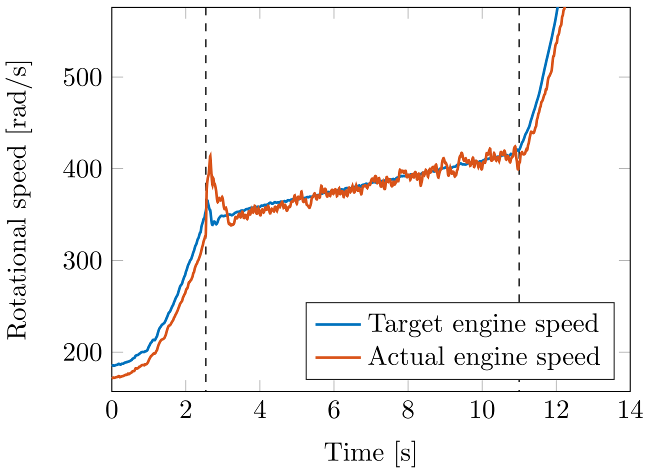

(c) Proposed ECU-based traction control.

Fig. 1. Experimental comparison of the proposed TCS.

These results show that ECU-based traction control offers substantial advantages compared to classical DCU-based TCSs. Performance can be improved further by an analytic control design based on input-output linearization.

[1] The target speed was estimated and drawn manually for reference in figure 1a, as the DCU-based TCS was available as blackbox only in the considered prototypical test vehicle.

5. CONCLUSION

We proposed a novel stability and passivity analysis of the zero dynamics of TCSs resulting from the input-output linearization of a 5-state longitudinal vehicle model including torsional dynamics of the drivetrain. This led to the first proof of global, exponential, parameter independent stability assuming a time-varying road adhesion coefficient. Furthermore, the ECU-based TCS was evaluated in a test vehicle and compared to both a DCU-based and an ECU-based benchmark TCS. The novel experimental validation showed, that the ECU-based TCS based on input-output linearization outperforms the other approaches in terms of tracking performance, disturbance attenuation and damping of drivetrain oscillations. This confirmed the robustness of the TCS with respect to parameter variations, as for example tires, vehicle load and environmental conditions were different to our previous work.

It can further be noted that the herein presented stability results can also directly be extended to the case of a 4WD drivetrain with on-demand torque bias systems, as proposed by Reichensdörfer et al. (2019). Therefore, the proposed method shows global, exponential stability for such vehicles as well. Also, it is interesting that exponential stability for time-varying road adhesion coefficients required only the mild assumption that the adhesion coefficient is bounded from below by a strictly positive value, while asymptotic stability required it only to be non-negative. However, this lower bound can be chosen arbitrarily close to zero and even for $\mu = 0$, at least asymptotic stability of the zero dynamics can still be guaranteed.

Future work could focus on more complex design models for the input-output linearization, including additional dynamics or on the reference speed generation for the ECU-based controller. Also, different control approaches for the linearized substitute system could be further investigated, as well as different reference models.

REFERENCES

Adamy, J. (2014). *Nichtlineare Systeme und Regelungen. 2., bearbeitete und erweiterte Auflage*. Springer, Berlin, 2 edition. In German.

Barabanov, N. (1988). On the Kalman problem. *Siberian Mathematical Journal*, 29(3), 333–341.

Byrnes, C.I. and Isidori, A. (1989). New results and examples in nonlinear feedback stabilization. *Systems & Control Letters*, 12(5), 437–442.

Chapuis, C., Bideaux, E., Brun, X., and Minoiu-Enache, N. (2013). Comparison of feedback linearization and flatness control for anti-slip regulation (ASR) of an hybrid vehicle: From theory to experimental results. In *2013 European Control Conference (ECC)*, 446–451. IEEE.

Fitts, R. (1966). Two counterexamples to Aizerman's conjecture. *IEEE Transactions on Automatic Control*, 11(3), 553–556.

Fujii, K. and Fujimoto, H. (2007). Traction control based on slip ratio estimation without detecting vehicle speed for electric vehicle. In *2007 Power Conversion Conference-Nagoya*, 688–693. IEEE.

Isidori, A. (1989). *Nonlinear Control Systems*. Springer, Berlin, 2 edition.

Ivanov, V., Savitski, D., and Shyrokau, B. (2015). A survey of traction control and antilock braking systems of full electric vehicles with individually controlled electric motors. *IEEE Transactions on Vehicular Technology*, 64(9), 3878–3896.

Jaime, R.P., Kästner, F., Erban, A., and Knödler, K. (2014). Algorithms for recuperation and traction in electric vehicles. *ATZelektronik worldwide*, 9(2), 4–9.

Khalil, H.K. (1996). *Nonlinear Systems*. Prentice-Hall, Englewood Cliffs, NJ, 3 edition.

König, L., Schindele, F., and Ghosh, J. (2019). ITC–model-based feed forward traction control. In *9th International Munich Chassis Symposium 2018*, 265–283. Springer.

Lur'e, A. and Postnikov, V. (1944). On the theory of stability of control systems. *Applied mathematics and mechanics*, 8(3), 246–248. In Russian.

Mousavi, A., Davaie-Markazi, A.H., and Masoudi, S. (2018). Comparison of adaptive fuzzy sliding-mode pulse width modulation control with common model-based nonlinear controllers for slip control in antilock braking systems. *Journal of Dynamic Systems, Measurement, and Control*, 140(1), 011014.

Nakakuki, T., Shen, T., and Tamura, K. (2008). Adaptive control approach to uncertain longitudinal tire slip in traction control of vehicles. *Asian Journal of Control*, 10(1), 67–73.

Nyandoro, O.T., Pedro, J.O., Dwolatzky, B., and Dahunsi, O.A. (2011). State feedback based linear slip control formulation for vehicular antilock braking system. In *Proceedings of the World Congress on Engineering*, volume 1.

Pacejka, H. (2005). *Tyre and vehicle dynamics*. Butterworth-Heinemann, Oxford, 2 edition.

Reichensdörfer, E., Degel, W., Odenthal, D., and Wollherr, D. (2019). Nonlinear traction control design, stability analysis and experiments for vehicles with on-demand 4WD torque bias systems. In *2019 IEEE 58th Conference on Decision and Control (CDC)*, 6669–6674. IEEE.

Reichensdörfer, E., Odenthal, D., and Wollherr, D. (2018). On the stability of nonlinear wheel-slip zero dynamics in traction control systems. *IEEE Transactions on Control Systems Technology*, 28(2), 489–504, 2020.

Rill, G. (2007). Wheel dynamics. In *Conference Proc. of the XII International Symposium on Dynamic Problems of Mechanics (DINAME), ABCM, Brasil*.

Zech, A., Eberl, T., Marx, C., and Müller, S. (2019). Analysis of the potential of a new control approach for traction control considering a P2-hybrid drivetrain. In *9th International Munich Chassis Symposium 2018*, 285–303. Springer.

Zech, A., Eberl, T., and Müller, S. (2017). Analyse einer neuen kaskadierten Reglerstruktur für die Antriebsschlupfbegrenzung hochdynamischer Fahrzeugantriebe. In *8. VDI/VDE Fachtagung, "AUTOREG 2017 - Automatisiertes Fahren und vernetzte Mobilität"*, volume 2292 of *VDI-Berichte*, 287–297. VDI-Verlag.

Zech, A., Eberl, T., Reichensdörfer, E., Odenthal, D., and Müller, S. (2018). Method for developing tire slip controllers regarding a new cascaded controller structure. In *14th International Symposium on Advanced Vehicle Control (AVEC)*, 302–307.